NMR-based structural biology enhanced by dynamic nuclear polarization at high magnetic field

12 AUTHORS, INCLUDING:

Eline J Koers
Utrecht University
14 PUBLICATIONS **125** CITATIONS

SEE PROFILE

Markus Weingarth
Utrecht University
30 PUBLICATIONS **471** CITATIONS

SEE PROFILE

Olivier Ouari
Aix-Marseille Université
82 PUBLICATIONS **1,402** CITATIONS

SEE PROFILE

Paul Tordo
Aix-Marseille Université
289 PUBLICATIONS **6,888** CITATIONS

SEE PROFILE

ARTICLE

NMR-based structural biology enhanced by dynamic nuclear polarization at high magnetic field

Eline J. Koers · Elwin A. W. van der Cruijsen · Melanie Rosay ·
Markus Weingarth · Alexander Prokofyev · Claire Sauvée ·
Olivier Ouari · Johan van der Zwan · Olaf Pongs · Paul Tordo ·
Werner E. Maas · Marc Baldus

Abstract Dynamic nuclear polarization (DNP) has become a powerful method to enhance spectroscopic sensitivity in the context of magnetic resonance imaging and nuclear magnetic resonance spectroscopy. We show that, compared to DNP at lower field (400 MHz/263 GHz), high field DNP (800 MHz/527 GHz) can significantly enhance spectral resolution and allows exploitation of the paramagnetic relaxation properties of DNP polarizing agents as direct structural probes under magic angle spinning conditions. Applied to a membrane-embedded K^+ channel, this approach allowed us to refine the membrane-embedded channel structure and revealed conformational substates that are present during two different stages of the channel gating cycle. High-field DNP thus offers atomic insight into the role of molecular plasticity during the course of biomolecular function in a complex cellular environment.

Keywords NMR · Dynamic nuclear polarization · Membrane · Protein · Solid-state NMR

E. J. Koers · E. A. W. van der Cruijsen · M. Weingarth ·
A. Prokofyev · J. van der Zwan · M. Baldus (✉)
NMR Spectroscopy, Bijvoet Center for Biomolecular Research,
Department of Chemistry, Faculty of Science, Utrecht
University, 3584 CH Utrecht, The Netherlands
e-mail: m.baldus@uu.nl

M. Rosay · W. E. Maas
Bruker BioSpin Corporation, 15 Fortune Drive, Billerica,
MA 01821, USA

A. Prokofyev · O. Pongs
Department of Physiology, Faculty of Medicine, Saarland
University, Building 56, 66421 Homburg, Germany

C. Sauvée · O. Ouari · P. Tordo
CNRS, ICR UMR 7273, Aix-Marseille Université,
13397 Marseille, France

Abbreviations

AT	Ambient temperature
DNP	Dynamic nuclear polarization
LT	Low temperature
MAS	Magic angle spinning
PRE	Paramagnetic relaxation enhancement
ssNMR	Solid-state nuclear magnetic resonance
TM	Transmembrane helix
MRI	Magnetic resonance imaging
SF	Selectivity filter
PDSD	Proton-driven spin diffusion
TOTAPOL	1-(TEMPO-4-oxy)-3-(TEMPO-4-amino)propan-2-ol
AMUPol	(15-{[(7-oxyl-3,11-dioxa-7-azadispiro[5.1.5.3]hexadec-15-yl)carbamoyl][2-(2,5,8,11-tetraoxatridecan-13-ylamino)}-[3,11-dioxa-7-azadispiro[5.1.5.3]hexadec-7-yl])oxidanyl

Introduction

Dynamic nuclear polarization (DNP, Overhauser 1953), a process in which nuclear spins are polarized via microwave

irradiation of a nearby electron spin, is finding widespread applications in nuclear magnetic resonance (NMR) spectroscopy (Hall et al. 1997; Ardenkjær-Larsen et al. 2003) and magnetic resonance imaging (MRI) (Gallagher et al. 2008; Cassidy et al. 2013). In solid-state NMR (ssNMR), the combined application of low-temperature (LT)-DNP, magic angle spinning (MAS, Ref. Andrew et al. 1958) and exogenous paramagnetic polarizing agents has been employed as a signal enhancement method with increasing applications in material (Rossini et al. 2013) and life sciences (Ni et al. 2013). For example, LT-DNP under MAS has been used to study membrane-associated peptides (Salnikov et al. 2010; Koers et al. 2013) as well as intermediate (Bajaj et al. 2009) and ligand-bound membrane protein states (Reggie et al. 2011; Linden et al. 2011b; Andreas et al. 2013). In addition, DNP-MAS has been successfully applied on cellular preparations (Renault et al. 2012b; Wang et al. 2013; Takahashi et al. 2013) and can be used to examine large macromolecular complexes (Gelis et al. 2013).

Paramagnetic agents are also widely employed to enhance contrast and resolution in MRI applications (Lauterbur 1973). The same principles have made paramagnetic relaxation enhancements (PREs) invaluable tools to refine molecular structures in biomolecular applications of solution (Bertini et al. 2005; Otting 2010) and, more recently, solid-state NMR (Buffy et al. 2003; Nadaud et al. 2007). In the latter case, elegant approaches have also been proposed to reduce spectroscopic repetition rates (Wickramasinghe et al. 2009) and it is well known that the modulation of longitudinal relaxation rates by PREs favorably influences the repetition rates of (LT)-DNP experiments.

While progress has been made in building DNP systems at high fields (Matsuki et al. 2010; Barnes et al. 2012), most commercially available DNP-NMR spectrometers have been operating at a ^{1}H resonance frequency of 400 MHz (and 263 GHz DNP) where spectroscopic studies, can be hampered by the comparatively low spectral resolution. Here, we investigate the use of MAS DNP instrumentation operating at 800 MHz/527 GHz for biomolecular solid-state NMR. We utilized uniformly (^{13}C, ^{15}N) and (^{2}H^{13}C^{15}N) labeled variants of the membrane embedded potassium channel KcsA as a model system. Both crystallographic information (Zhou et al. 2001; Uysal et al. 2009) as well as ssNMR data are available (Ader et al. 2008; Schneider et al. 2008; Bhate et al. 2010; van der Cruijsen et al. 2013) for KcsA. To regulate the conduction of potassium ions through the pore of the channel, KcsA comprises two coupled gates that are located at either end of the channel pore and that are called the activation and inactivation (a.k.a. selectivity filter, SF) gate. Channel inactivation leads to a collapse of the SF and opening of the activation gate (Ader et al. 2009a, b; Cuello et al. 2010a).

Starting with the closed conductive channel state that has been well characterized by X-ray and ssNMR, we examined the influence of transversal PREs and conformational heterogeneity upon LT-DNP spectra obtained at 800 MHz/527 GHz at the residue-specific level. Our NMR studies were assisted by single channel measurements and MD calculations. Furthermore we compared spectral resolution and DNP enhancements to results obtained at 400 MHz (DNP) and 700 MHz, providing insight into site-specific origin for ssNMR line broadening and signal enhancement under LT-DNP conditions. For many ion channel residues, we observed an increase in spectral resolution. These findings provided the basis to employ high-field DNP to examine how variations in ion channel structure correlate to the channel state before and after inactivation.

Materials and methods

Sample preparation

We prepared proteoliposomal samples containing uniformly (^{13}C, ^{15}N) labelled KcsA in the closed conductive and open inactivated state as described before (Ader et al. 2008; van der Cruijsen et al. 2013). As in Ref. (Weingarth et al. 2014), uniformly (^{2}H, ^{13}C, ^{15}N) labeled KcsA was expressed, back exchanged and reconstituted in asolectin (Sigma). For DNP-based ssNMR experiments, we washed liposomal KcsA samples with 50 μL DNP solution containing TOTAPOL (5 mM as well as 10 mM) or AMUPol (25 mM) in 1:2:2 (v/v/v) glycerol-d8 (Cortecnet), D$_2$O, and H$_2$O with buffer conditions at pH 7; 50 mM NaPi, 50 mM NaCl, 50 mM KCl and for pH 4 or 3.5; 10 mM Na$_3$ citrate, 120 mM NaCl. Radical concentrations (5 mM TOTAPOL, 25 mM AMUPol) were chosen such that PREs were comparable (see SI Table 1 and 2). A 10 mM TOTAPOL concentration was chosen to study the influence of the radical concentration on linewidth and enhancement. Samples were subsequently centrifuged at 125,000g for approximately 30 min followed by removal of the supernatant. This procedure was done twice. The final pellet was then transferred from the Eppendorf tube to a 3.2 mm sapphire rotor by means of a funnel and centrifugation for 5–10 s in a bench top centrifuge.

Solid-state NMR and DNP experiments

ssNMR and DNP experiments were conducted using 3.2 mm triple-resonance (^{1}H,^{13}C,^{15}N) MAS probe heads at static magnetic fields ranging from 9.4 to 18.8 T corresponding to proton/electron resonance frequencies of 400 MHz/263 GHz (Rosay et al. 2010), 700 or 800 MHz/

527 GHz (Bruker BioSpin). Data were recorded at 100 K (LT) and at 273 K (referred to as ambient temperature, AT) employing MAS rates between 8 and 15 kHz. Pulse schemes reflected standard homonuclear proton-driven spin diffusion (PDSD) and double-quantum filtered (^{13}C, ^{13}C) using SPC-5 recoupling (Hohwy et al. 1999). NCA experiments typically utilized SPECIFIC-CP transfer (Baldus et al. 1998) (see SI for further details on the experimental parameters).

Molecular dynamics simulations

Atomistic MD simulations were carried out using the GROMACS simulations package version 4.5.3 with the GROMOS53a6 force field (Soares et al. 2005). The starting structure was derived from crystal structure PDB code 3EFF (Uysal et al. 2009) truncated to residues 22–115. The channel was embedded in a POPG bilayer in an aqueous solution of 150 mM KCl. All simulations were carried out under constant 1 bar pressure and 283 K temperature. The chemical shift analysis presented in Fig. 3 is based on a 10 ns simulation, while chemical shifts where predicted every 200 ps using SPARTA+ (Shen and Bax 2010). Residue-specific bulk water distances were measured with the GROMACS tool g_mindist.

Single channel measurements

Single channel recordings of KcsA were performed on a planar lipid bilayer setup (Compact, Ionovation GmbH). Asolectin lipid bilayers were formed by painting the lipids dissolved in n-decane over a 200 μm hole in a Teflon-septum that separated two chambers, cis and trans. 1–5 μL KcsA proteoliposomes were added to the cis chamber. Single channel currents were recorded in symmetrical 150 mM KCl solution. The cis side was buffered to pH 7.0 by 10 mM HEPES and trans side was buffered to pH 4.0 by 10 mM succinic acid. All measurements were performed at room temperature. Data were sampled at 10 kHz and filtered at 1 kHz.

Results and discussion

Paramagnetic relaxation effects

To investigate paramagnetic relaxation effects in our DNP samples, we firstly studied membrane-embedded uniformly (^{13}C, ^{15}N) labeled KcsA at AT before (Fig. 1a, black) and after addition of 5 mM TOTAPOL and 20 % glycerol (Fig. 1a, green). Note that this situation (employing water-soluble radicals) is different from using covalently attached radicals (see, e.g., Ref. Sengupta et al. 2012). Addition of
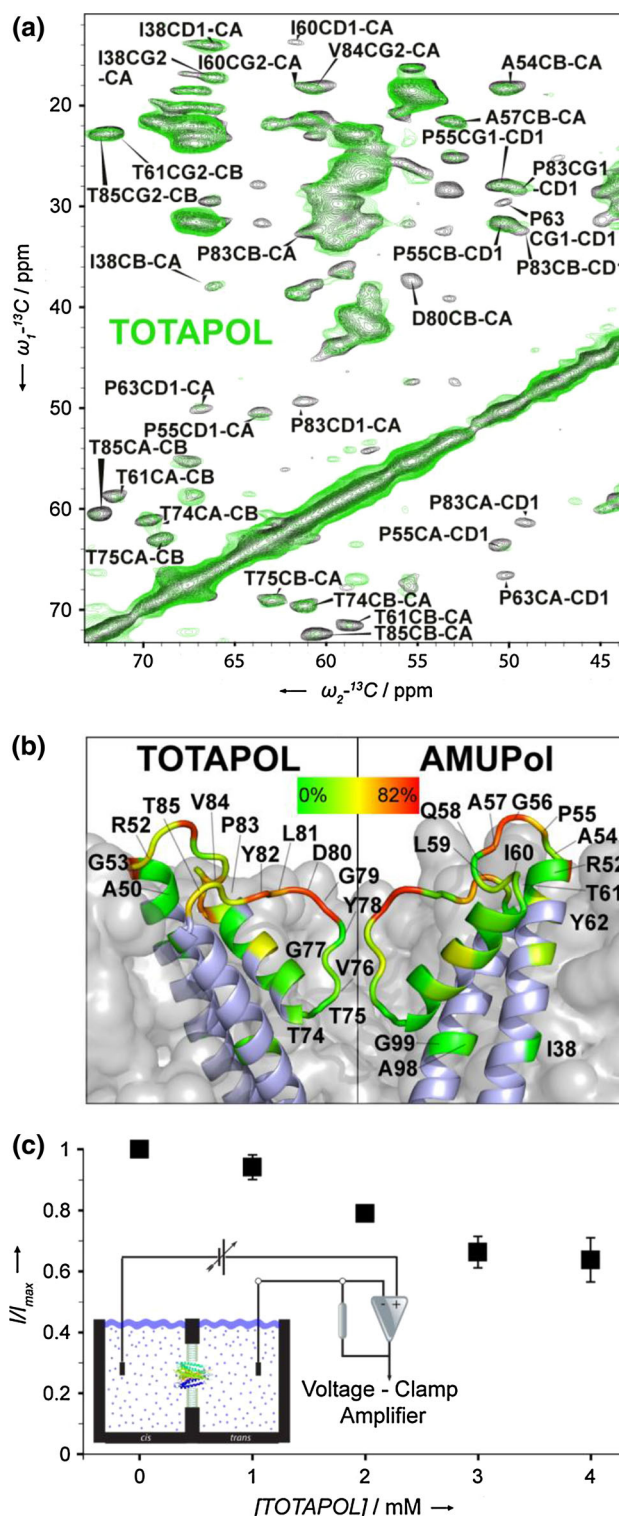

Fig. 1 **a** (^{13}C, ^{13}C) PDSD data obtained at AT conditions before (*black*) or after addition of 5 mM TOTAPOL (*green*). In **b**, the residue-specific signal attenuation due to the addition of 5 mM TOTAPOL and 25 mM AMUPol is shown. The *scale bar* represents signal scaling after addition of biradical ranging from 0 (*green*) to 82 % (*red*). Experimental parameters are given in the Supporting Information. **c** Single channel current of KcsA in planar lipid bilayers at increasing concentration of TOTAPOL

the biradical left large parts of the spectra unaffected (i.e. no reduction of signal intensity and chemical shift changes) except for, e.g., backbone resonances of Pro 63, Thr 61 or Thr 85 or side-chain cross peaks of Val 84 (Fig. 1a). Assignments indicated in Fig. 1 (black) and utilized in the same color coding throughout this work are based on our previous studies on KcsA variants (Schneider et al. 2008; van der Cruijsen et al. 2013). PRE-induced signal modulations were exclusively found in the solvent-exposed regions (Supporting Table I) as can be deduced from the attenuation plotted on a three-dimensional membrane embedded model of KcsA in the closed conductive state (Fig. 1b, left). We note that because of the lack of assignments and insufficient spectral resolution in our 2D data, we were not able to track the C-terminal region of KcsA that is solvent exposed. Within the selectivity filter (SF, residues 74–79) which also comprises the inactivation gate (Ader et al. 2008), we observed a strong decrease in PREs when moving from the water-exposed entry side (Gly 79) down towards the center of the channel (Thr 74). Signal intensities for many solvent-exposed residues were reduced by more than a factor of 5 (Fig. 1b, left, red). Most likely, variations of solvent PREs (Hocking et al. 2013) on the protein-solvent interface are caused by similar mechanisms as found for the radical TEMPOL in earlier solution state NMR experiments (Esposito et al. 1992; Pintacuda and Otting 2002; Bernini et al. 2006). Hence, our results suggest that PREs at AT are restricted to a few Angstrom below the solvent exposed channel parts caused by radicals residing in the solvent or close to the solvent-exposed protein surface. Additional experiments (data not shown) suggested that the addition of glycerol does not lead to additional line broadening at AT.

Since strong PREs were found at the extracellular channel pore entrance, we investigated TOTAPOL effects on KcsA channel activity by electrophysiological experiments (Fig. 1c). Concentrations as low as 4 mM TOTAPOL affect single channel properties of KcsA by reducing amplitudes of the single channel current by as much as 40 % at which point a plateau is reached. The latter excludes the possibility of channel blockage by the radical. Instead, these results suggest, together with the lack of chemical shift changes (Fig. 1a), a partial occlusion of the channel entry with increasing concentrations of the biradical without perturbing the structure of the channel itself. We note that weak transient binding cannot be excluded.

Next we conducted experiments using 25 mM AMUPol which revealed a similar overall relaxation profile (Fig. 1b, right), albeit with slightly weaker effects at the channel entry (Supporting Table 2 and Fig. S1). These results suggest that PREs at AT are slightly larger for KcsA samples prepared with 5 mM TOTAPOL than in samples containing 25 mM AMUPol. This observation would be consistent with the influence of different molecular sizes of the two biradicals considered. Due to the additional hydrophilic tail of AMUPol and the size of the molecule, the radical center of AMUPol would be, on average, further distant to the protein—lipid surface than in the case of the more hydrophobic TOTAPOL.

Intrinsic linewidth at low temperature

Our previous analysis identifies PREs as an important source of T_2 relaxation that provides direct insight into the solvent-exposed molecular region (Fig. 1b). In addition, molecular motion should give rise to structural disorder at lower temperatures. Such effects have, for example, been exploited in the context of studying peptide and protein folding by ssNMR (Havlin and Tycko 2005; Heise et al. 2005). More recently, the dynamics of globular proteins (Linden et al. 2011a) and the impact of solvent dynamics for LT ssNMR experiments have been investigated (Siemer et al. 2012). In the following, we hence considered contributions of both PREs and structural disorder for LT-DNP data obtained at 800 MHz/527 GHz under variable biradical concentration and compared our results to experiments at 400 MHz DNP conditions.

Figure 2 compares results of a standard 2D (^{13}C, ^{13}C) PDSD experiment obtained on uniformly (^{13}C, ^{15}N) labeled KcsA in asolectin bilayers at 400 MHz (black) and 800 MHz (red) under DNP conditions using TOTAPOL as polarizing agent. At the latter field strength, we also compared data for a TOTAPOL concentration of 5 mM (Fig. 3, black) and 10 mM (Fig. 3, orange) and focused on residues around the selectivity filter. In order to obtain complementary insight into the role of residue-specific channel motion we conducted molecular dynamics (MD) simulations and computed the chemical-shift distribution (Fig. 3, histograms) from our MD trajectories as shown before (Heise et al. 2005; Zachariae et al. 2008). In detail, we used standard CS prediction programs to translate backbone fluctuations obtained from the MD trajectory to backbone chemical shift variations. The resulting histograms were compared to our experimental results at 100 K, where backbone motions should be largely frozen out. We observed a remarkable correlation between linewidths determined experimentally and predicted from MD runs for the residues Gly 77, Thr 74 and Thr 75 (Fig. 3, see also Supporting Table 3). Note that this analysis suggests that structural disorder in the selectivity filter is restricted to Thr 74 that exhibits a significantly larger line width than Thr 75 and Gly 77 (vide infra) and only mildly improves in resolution when moving from 400 to 800 MHz (Fig. 2c).

The other two residues investigated, i.e., Thr 85 and Gly 79, exhibit a greater linewidth than predicted by the MD
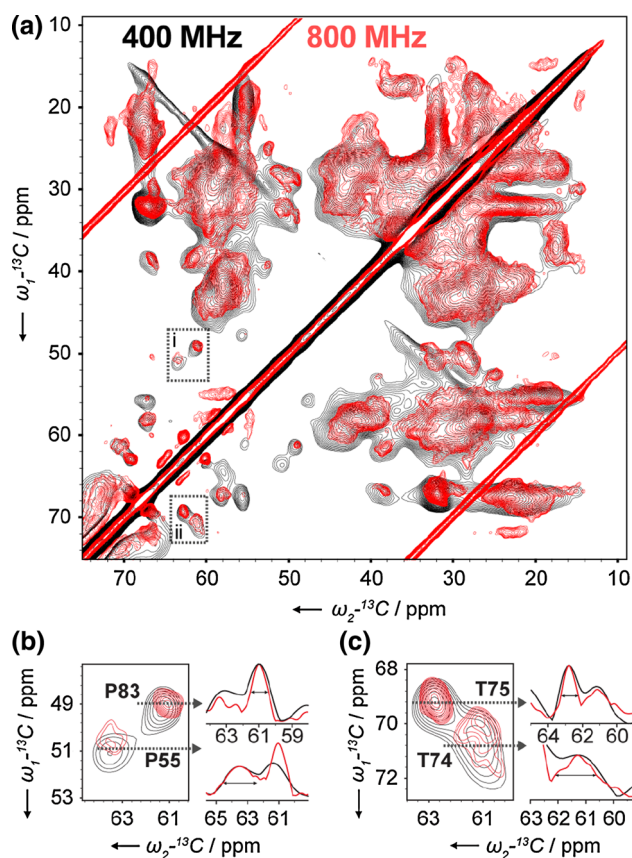
Fig. 2 a 400 and 800 MHz DNP 2D PDSD spectra recorded at 400 (*black*) and 800 MHz (*red*) are overlayed. Proline CD1-CA (**b**) and threonine CB–CA (**c**) regions are shown, together with 1D projections (as defined in topspin) of the CA peaks in the direct dimension on the *right*. Note that the 400 MHz DNP 2D PDSD spectrum contains an MAS sideband that is folded in

simulation data (Fig. 3). These residues were among the most attenuated ones at AT (Fig. 1), suggesting that here broadening is mainly due to paramagnetic relaxation. This view is further supported by investigating the effect of increasing the concentration of TOTAPOL from 5 to 10 mM. In this case, broadening for Thr 85 and G79 further strongly increases while PREs for Thr 74, Thr 75 and Gly 77 remained limited (Fig. 3). Notably, residues that seem to be dominated by PREs such as Pro 83 still exhibit an improvement in spectral resolution at higher field (Fig. 2b). Taken together, our analysis confirms that line broadening effects at low temperatures can be explained by two phenomena: conformational heterogeneity and paramagnetic relaxation effects.

Comparison to high field data at AT

To further verify our conclusions regarding the intrinsic line width under 800 MHz DNP conditions, we compared our LT-DNP data (Figs. 4, 5, red) to results obtained at AT

conditions in the absence of the two biradicals of interest (Figs. 4, 5, black). The latter data were obtained at lower field strength (700 MHz). We analyzed 2D PDSD experiments at LT (Fig. 4) as well LT NCA data under DNP conditions using 5 mM TOTAPOL (Fig. 5a) and 25 mM AMUPol (Fig. 5b). In both sets of experiments we observed PRE modulated signal intensities for residues located at the channel-water interface. For example, Thr 61 and Thr 85 exhibited weaker signal intensities than Thr 74 and Thr 75. Note that these findings were made irrespective of the biradical type. We note that additional correlations in the region 70–65 ppm in Fig. 4 stem from co-purified lipids which are mobile under AT conditions (Weingarth et al. 2013). On the other hand, the apparent linewidth of many backbone Cα–Cβ (Fig. 4) or N–Cα (Fig. 5) correlations seen at LT-DNP in the presence (Fig. 4a) or absence (Fig. 4b, blue) of microwave irradiation compared favorably to data obtained at high temperatures. For example, LT-DNP correlations seen for Thr 74 or Gly 77 are virtually identical to data seen at AT 700 MHz conditions. In the case of Gly 79, we previously had detected increased channel dynamics (Ader et al. 2010). The observed weak intensity at LT conditions can hence be explained by a combination of increased dynamics (vide infra) and PREs.

Overall and residue specific enhancements

Firstly, we determined DNP enhancement factors at 800 MHz/527 GHz conditions using one-dimensional ^{13}C CP experiments for both protonated and deuterated variants of membrane-embedded KcsA. We observed DNP enhancements of 2.8 and up to 8.3 for uniformly (^{1}H, ^{13}C, ^{15}N) labeled KcsA with 5 mM TOTAPOL and 25 mM AMUPol, respectively. Similar values were obtained for one-dimensional ^{15}N CP experiments. In the case of AM-UPol, enhancement factors had dropped to 5 when remeasured after 5 months storage at 193 K (Fig. 6, colored bars). Compared to equivalent experiments conducted at 400 MHz, the 5 mM TOTAPOL sample hence showed an approximately four-fold decrease in DNP enhancement at 800 MHz/527 GHz. When comparing LT-DNP ssNMR data (Fig. 5a, b) to AT ssNMR experiments (Fig. 5a, b) on uniformly (^{1}H, ^{13}C, ^{15}N) labeled KcsA, the addition of 25 mM AMUPol resulted in a sizable increase in signal to noise per hour by a factor of 6.9 (SI Fig. S2). Deuteration and ^{1}H back exchange for (^{2}H, ^{13}C, ^{15}N) labeled KcsA further increased DNP enhancements from 8.3 to 13.2 which is in line with earlier work (Kagawa et al. 2009; Akbey et al. 2010). Clearly, the enhancements seen at 800 MHz are lower than for data obtained at 400 MHz conditions. However, DNP enhancement factors reported in the literature (Salnikov et al. 2010; Reggie et al. 2011;
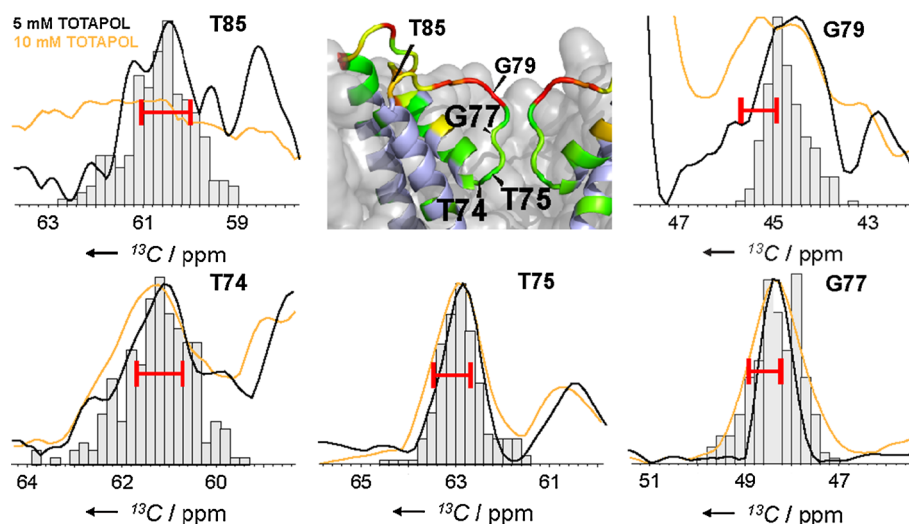
Fig. 3 Projections of resolved peaks stemming from selectivity filter residues. 1D projections using 5 mM TOTAPOL (*black*) and 10 mM TOTAPOL (*orange*) are overlayed with the chemical shift distribution predicted by MD (see experimental details). For reference, the line width measured at 700 MHz AT, without addition of TOTAPOL is given by *red bars*. Results from G79, G77, T74 and T75 were taken from an NCA spectrum and T85 was determined from a (^{13}C, ^{13}C) PDSD spectrum. The *inset* structure is a zoom-in from Fig. 1b (solvent PREs at AT). Experimental parameters are given in the Supporting Information and *line shape* fitting parameters can be found in Supporting Table 3
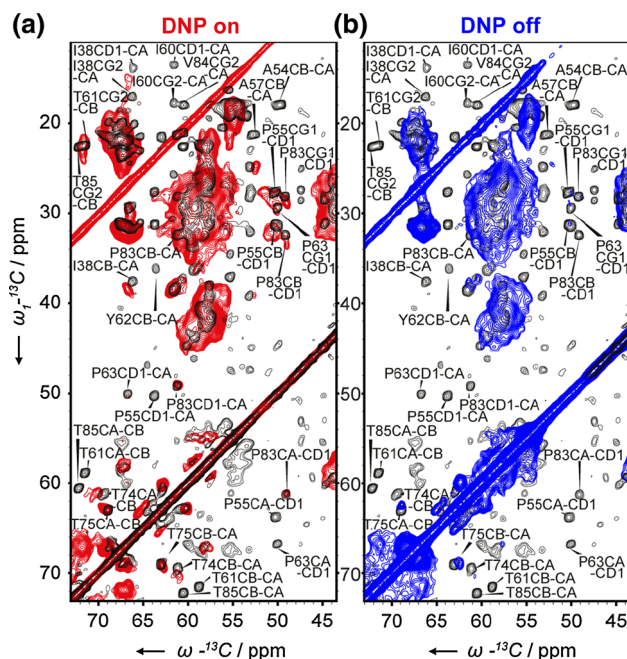

Fig. 4 Overlay of (^{13}C, ^{13}C) PDSD at 700 MHz, 273 K without radicals (*black*) and 800 MHz LT, 5 mM TOTAPOL with (**a**, *red*) and without microwaves (**b**, *blue*). Experimental parameters are given in the Supporting Information

Linden et al. 2011b; Jacso et al. 2012; Renault et al. 2012a; Andreas et al. 2013; Koers et al. 2013) for membrane proteins at 400 MHz and 100 K vary considerably in range from 8 to 32. These observations point to an important influence of the sample preparation upon the LT-DNP performance.

The favorable spectral resolution at 800 MHz and the observed signal modulation due to PREs and motional effects prompted us to determine *residue-specific* DNP enhancements at 800 MHz/527 GHz. In Fig. 6, this analysis is presented for our uniformly (^{1}H, ^{13}C, ^{15}N) labeled KcsA samples. To visualize the effect of the distance of the AMUPol or TOTAPOL radical to the nearest position possible to the channel, we plotted PREs obtained at AT and residue-specific DNP enhancements against the distance to the nearest bulk water taken from the MD simulations (Fig. 6a–d). As expected from the Solomon-Bloembergen equations (Solomon 1955; Bloembergen and Morgan 1961), residues located closer to the surface exhibited stronger signal attenuation. Especially at the lower biradical concentration, residue-specific variations are however, substantial and most likely relate to local shielding effects by lipid-protein interactions for residues such as Tyr 45, Ala 50-Arg 52 or Trp 87 (dashed box in Fig. 6a) which are all located at the protein-lipid interface (see. Figure 1b, left). Moreover, a uniform biradical distribution may only be established at concentrations higher than 5 mM TOTAPOL.

Both effects may also explain the larger fluctuations in residue-specific DNP enhancements with maximum enhancements seen for Gly 77, Ile 38, Thr 75 and Pro 83 in the 5 mM TOTAPOL sample (Fig. 6c). The most dramatic difference is found for Gly 77. Both in the 5 mM TOTAPOL sample and the (^{2}H^{13}C^{15}N) 25 mM AMUPol sample this residue exhibits the highest residue specific enhancement, as shown in red in the structures of Fig. 7, relative to the values seen in 1D data (Fig. 6c, Table S4).
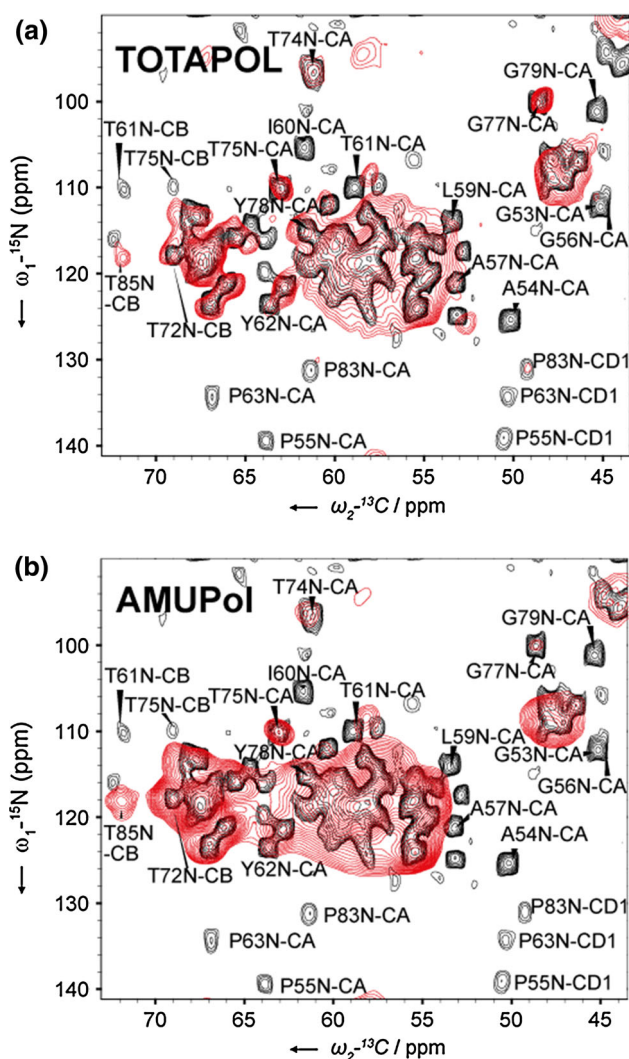
Fig. 5 Comparison of KcsA data obtained at AT and LT-DNP conditions. The results of 2D NCA experiments obtained at 700 MHz at AT conditions and without biradical (*black*) are compared to data acquired under DNP conditions (*red*) at 800 MHz/527 GHz using 5 mM TOTAPOL (**a**) or 25 mM AMUPol (**b**). Experimental parameters are given in the Supporting Information

We note that for the deuterated case, spectra without microwave irradiation suffered from limited signal to noise and an analysis such as shown in Fig. 6 was restricted to a smaller number of protein residues around the channel pore segment (see Supporting Table 4). In this protein region, variations in DNP enhancements are small compared to the PREs seen at AT which would be consistent with the dominant influence of spin diffusion (van der Wel et al. 2006). Strong variations were only observed for Gly 77 that is not only located at the center of the selectivity filter and thereby distant from both the solvent or cavity water but it is also surrounded by nearby potassium ions in crystal structures (Cuello et al. 2010b) (vide infra).

Residue-specific disorder before and after channel inactivation

Channel inactivation in KcsA is controlled by structural changes at the selectivity filter (the inactivation gate) and by a large hinged motion around the inner helix bundle (the activation gate). A complex kinetic behavior referred to as model gating underlies the concerted conformational changes at the inactivation and activation gate. Most likely, the kinetics reflect a combination of different channel populations associated with local fluctuations in channel structure. An understanding of these processes is still limited (Chakrapani et al. 2011). With our 800 MHz DNP setup, we studied the channel in the closed-conductive (Figs. 3, 4, 5, 6, 8a, c, zoom in) and open-inactivated (Fig. 8d–g, zoom in) conformation to be able to compare conformations of the selectivity filter in both states. In the closed-conductive state, we analyzed 2D CC (Fig. 8c) and NC spectra (Fig. 8b) both at AT (black) and LT-DNP (red) conditions.

We observed that the peak of residue Thr 74 at the lower part of the selectivity filter (indicated in red in Fig. 8a, spectrum Fig. 8c) is broadened by a higher degree of structural heterogeneity (see also Fig. 3) compared to residues such as Thr 75 and Gly 77 that are located towards the center of the selectivity filter (Fig. 8a, blue). Our results obtained on the closed-conductive state of KcsA hence suggested that residue-specific channel dynamics lead to local disorder under LT-DNP conditions.

We then compared our findings of Fig. 8a–c to the channel conformation after inactivation that can be induced by lowering pH and by reducing K^+ concentrations below 20 mM (Ader et al. 2009a; van der Cruijsen et al. 2013) (Fig. 8e–g). Spectra recorded at AT conditions are shown in black and LT-DNP in green. In line with our earlier studies on the closely related KcsA-Kv1.3 channel (Ader et al. 2008, 2009a), we observed chemical shift changes in the selectivity filter. Compared to the AT data (black, Fig. 8e–g), we now however detected signal attenuation for Thr 75 at LT-DNP conditions (Fig. 8g, green) that was clearly visible before inactivation (Fig. 8c), i.e., in the closed conductive state. Interestingly, Thr 74 now is readily apparent in the open inactivated state. In contrast to the change in dynamics at the lower part of the SF, the upper part of the SF showed no change in dynamics. We can conclude by the clear appearance of residue Gly 77 before (Fig. 8b) and after inactivation (Fig. 8f) that in both states this residue showed no structural disorder. Notably, the same residue exhibited the strongest DNP enhancements (Figs. 6, 7). SF residues towards the extracellular side could not be examined due to PREs, e.g. residue Gly 79 of the SF remained attenuated (Figs. 1b, 8b).

Fig. 6 Residue specific solvent PRE attenuation at AT (**a**, **b**) and DNP enhancements (**c**, **d**) of KcsA with 5 mM TOTAPOL (**a**, **c**) and 25 mM AMUPol (**b**, **d**) as a function of the distance to the nearest bulk water. *Dashed arrows* are shown for *error bars* lacking upper boundaries. *Horizontal, dashed lines* indicate the DNP enhancements derived from 1D ^{13}C CP experiments. The *boxed area* in **a** contains residues Tyr 45, Ala 50, Glu 51, Arg 52, Trp 87 and Tyr 78. All, but Tyr 78 are part of the protein-lipid-water interface. We note the DNP enhancements using AMUPol and protonated KcsA had dropped to 5 after long term storage (see main text)
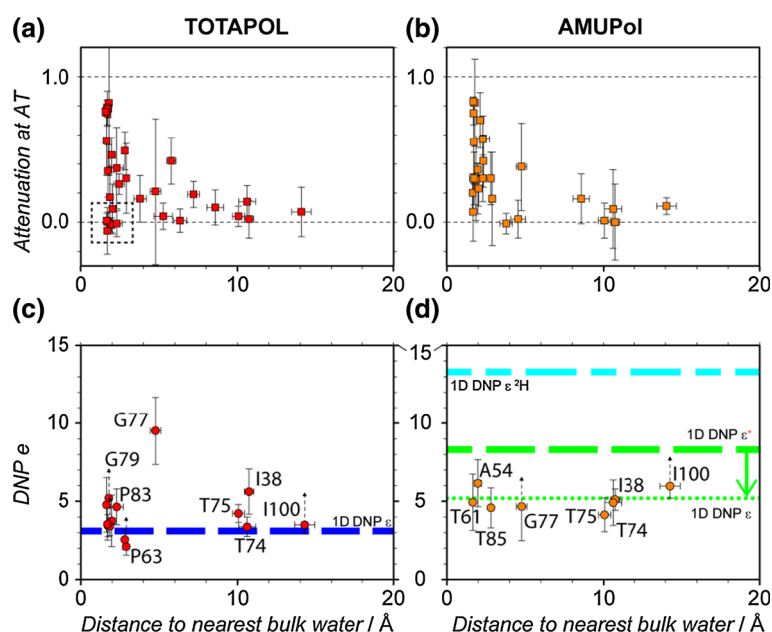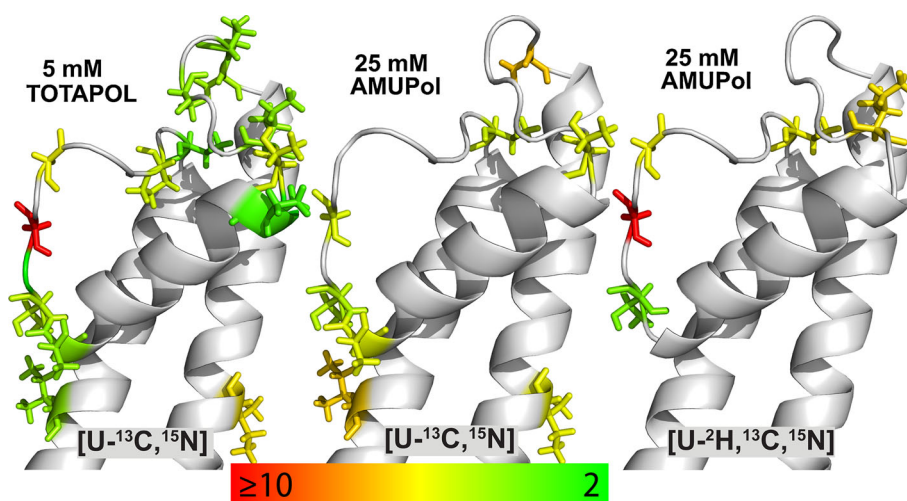

Fig. 7 Residue-specific LT-DNP enhancements in a close up region around the selectivity filter with (*left*) 5 mM TOTAPOL, (*middle*) 25 mM AMUPol, both uniformly (^{1}H, ^{13}C, ^{15}N) labeled KcsA, and (*right*) 25 mM AMUPol with proton back-exchanged uniformly (^{2}H, ^{13}C, ^{15}N) labeled KcsA. *Scale bar* refers to relative DNP enhancements ranging from 2 (*green*) to ≥10 (*red*)

In the open-inactivated state under LT-DNP conditions, we also observed peak doubling at Thr 101 (Fig. 8e, green) which is situated at the gating hinge of the activation gate. This residue exhibits a well characterized ssNMR chemical shift change (Ader et al. 2008, 2009a) as a result of opening of the activation gate (Fig. 8d). Note that these observations were insensitive to changes to stronger acidic pH in our proteoliposomal preparations (SI Fig. S4c). To understand the nature of the peak doubling observed at Thr 101, we investigated whether changes in activation gate opening

as seen in KcsA mutant crystals would lead to chemical-shift variations in our ssNMR spectra. Crystal structures of constitutively open KcsA mutants had revealed various degrees of activation gate opening ranging from 23 to 32 Å (Cuello et al. 2010b). Indeed, when comparing ^{13}Cα, and ^{15}N chemical shift predictions for open mutants forms between 23 and 32 Å, the size and trend in chemical shift variations were in remarkable agreement with our experimental results (SI Fig. S4). Assuming that the ssNMR signal intensity reports on the relative population of these
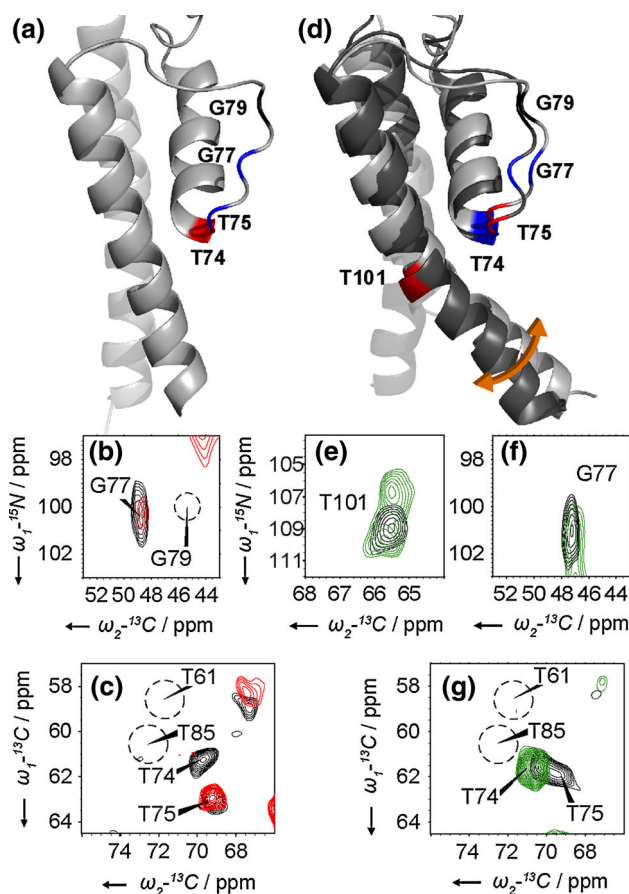
Fig. 8 Comparison of AT (*black*) and LT-DNP (*red/green*) ssNMR before (**a–c**) and after inactivation (**d–g**). **a** and **d** structures are taken from Ref. (van der Cruijsen et al. 2013) and (Cuello et al. 2010b). Channel residues that are apparent in the LT spectra are given in *blue* on the KcsA structure. Residues that disappear or exhibit strong line broadening at LT are indicated in *red*. In **d** two channel conformations (referring to an activation gate opening of 23 and 32 Å, respectively), that are most compatible with the ssNMR data are overlayed. **b** and **c** represent zoom-ins from Figs. 4a and 5 respectively. For complete spectra and further experimental details, see Supporting Information

opening events, our ssNMR data would be most compatible with the dominant contribution of two channel conformations: one species that only exhibits a limited opening (23 Å) and a second population that displays are fully open activation gate (32 Å) in our ssNMR spectra. These results would be consistent with structural fluctuations of the activation gate even under strongly acidic pH conditions where the activation gate is fully open (Chakrapani et al. 2007).

Conclusions

Dynamic nuclear polarization has become a powerful method to enhance spectroscopic sensitivities in the context of NMR and MRI. On the other hand, the availability of standard high-field NMR instruments has greatly enhanced the possibility to study complex (bio)molecular systems where spectral resolution is critical. We have shown that, compared to studies at 400 MHz, high field DNP significantly enhances the prospects to conduct in-depth structural investigations of complex molecules such as membrane proteins in different functional states.

We have demonstrated that these high field conditions can enhance spectral resolution. We also showed that the intrinsic paramagnetic properties of the polarizing agents can be used as direct structural probes during the spectroscopic analysis. In the case of the membrane embedded KcsA channel, our results help to pinpoint the water accessible pore of the channel in membranes. The most solvent-exposed surface shell exhibits strong PREs, at least under the conditions used in our experiments. We suspect that similar processes are also present in the context of material science applications.

The comparison of DNP data to results obtained at ambient temperatures furthermore allowed us to obtain insight into the role of ion channel plasticity before and after inactivation. This flexibility could be closely related to modal gating that represents an effective regulatory mechanism by which ion channels control the extent and time course of ionic fluxes. Our experiments identified specific selectivity filter residues that exhibit conformational flexibility before (Thr 74) and after inactivation (Thr 75, Thr 101). These observations underline that both gates are coupled (Ader et al. 2009a; Cuello et al. 2010a) and support emerging views (Chakrapani et al. 2011; Weingarth et al. 2014) that small structural fluctuations of the filter backbone can have drastic effects on gating changes. Compared to earlier DNP studies that were mostly conducted at 400 MHz, we find reduced overall signal enhancements at 800 MHz DNP conditions. This reduction is higher than predicted from theoretical studies (Hu et al. 2011) but it is in line with recent studies of AMUPol at lower magnetic fields (Sauvee et al. 2013; Fricke et al. 2013). As discussed before, the actual signal enhancements may also depend on the details of the sample conditions. For further studies on this subject, the membrane-embedded KcsA channel for which ssNMR resonance assignments as well as structural data are available (Schneider et al. 2008; van der Cruijsen et al. 2013) may represent a valuable experimental reference.

In parallel, further optimizations of the instrumental details including the use of lower temperatures (Barnes et al. 2012) or of pulsed DNP setups (Smith et al. 2012) may greatly improve DNP enhancements at high magnetic field. Moreover, our results using AMUPol and deuterated KcsA versions indicate that modifications of the polarizing agent (see, e.g., Ref. Zagdoun et al. 2013a) or of the proton

density of the target molecule itself (Kagawa et al. 2009; Akbey et al. 2010; Maly et al. 2012; Zagdoun et al. 2013b) additionally enhance the potential of DNP-supported structural biology. Note that in such studies reference data obtained using conventional NMR setups that we here used to examine the high field DNP performance and the details of the PRE mechanism would not be required. These considerations provide additional opportunities for in-depth studies of the conformational landscape that describes the workings of complex (bio)molecules using high field DNP technology.

References

Ader C, Schneider R, Hornig S et al (2008) A structural link between inactivation and block of a K + channel. Nat Struct Mol Biol 15:605–612. doi:10.1038/nsmb.1430

Ader C, Schneider R, Hornig S et al (2009a) Coupling of activation and inactivation gate in a K + -channel: potassium and ligand sensitivity. EMBO J 28:2825–2834. doi:10.1038/emboj.2009.218

Ader C, Schneider R, Seidel K et al (2009b) Structural rearrangements of membrane proteins probed by water-edited solid-state NMR spectroscopy. J Am Chem Soc 131:170–176. doi:10.1021/ja806306e

Ader C, Pongs O, Becker S, Baldus M (2010) Protein dynamics detected in a membrane-embedded potassium channel using two-dimensional solid-state NMR spectroscopy. Biochim Biophys Acta-Biomembr 1798:286–290. doi:10.1016/j.bbamem.2009.06.023

Akbey Ü, Franks WT, Linden A et al (2010) Dynamic nuclear polarization of deuterated proteins. Angew Chem Int Ed 49:7803–7806. doi:10.1002/anie.201002044

Andreas LB, Barnes AB, Corzilius B et al (2013) Dynamic nuclear polarization study of inhibitor binding to the M218-60 proton transporter from influenza A. Biochemistry 52:2774–2782. doi:10.1021/bi400150x

Andrew ER, Bradbury A, Eades RG (1958) Nuclear magnetic resonance spectra from a crystal rotated at high speed. Nature 182:1659

Ardenkjær-Larsen JH, Fridlund B, Gram A et al (2003) Increase in signal-to-noise ratio of > 10,000 times in liquid-state NMR. Proc Natl Acad Sci 100:10158–10163

Bajaj VS, Mak-Jurkauskas ML, Belenky M et al (2009) Functional and shunt states of bacteriorhodopsin resolved by 250 GHz dynamic nuclear polarization-enhanced solid-state NMR. Proc Natl Acad Sci USA 106:9244–9249. doi:10.1073/pnas.0900908106

Baldus M, Petkova AT, Herzfeld J, Griffin RG (1998) Cross polarization in the tilted frame: assignment and spectral simplification in heteronuclear spin systems. Mol Phys 95:1197–1207

Barnes AB, Markhasin E, Daviso E et al (2012) Dynamic nuclear polarization at 700 MHz/460GHz. J Mag Reson 224:1–7. doi:10.1016/j.jmr.2012.08.002

Bernini A, Spiga O, Venditti V et al (2006) NMR studies of lysozyme surface accessibility by using different paramagnetic relaxation probes. J Am Chem Soc 128:9290–9291. doi:10.1021/ja062109y

Bertini I, Luchinat C, Parigi G, Pierattelli R (2005) NMR spectroscopy of paramagnetic metalloproteins. ChemBioChem 6:1536–1549. doi:10.1002/cbic.200500124

Bhate MP, Wylie BJ, Tian L, McDermott AE (2010) Conformational dynamics in the selectivity filter of KcsA in response to potassium ion concentration. J Mol Biol 401:155–166. doi:10.1016/j.jmb.2010.06.031

Bloembergen N, Morgan LO (1961) Proton relaxation times in paramagnetic solutions. Effects of electron spin relaxation. J Chem Phys 34:842. doi:10.1063/1.1731684

Buffy JJ, Hong T, Yamaguchi S et al (2003) Solid-state NMR investigation of the depth of insertion of protegrin-1 in lipid bilayers using paramagnetic Mn2. Biophys J 85:2363–2373. doi:10.1016/S0006-3495(03)74660-8

Cassidy MC, Chan HR, Ross BD et al (2013) In vivo magnetic resonance imaging of hyperpolarized silicon particles. Nat Nanotechnol 8:363–368. doi:10.1038/nnano.2013.65

Chakrapani S, Cordero-Morales JF, Perozo E (2007) A quantitative description of KcsA gating II: single-channel currents. J Gen Physiol 130:479–496. doi:10.1085/jgp.200709844

Chakrapani S, Cordero-Morales JF, Jogini V et al (2011) On the structural basis of modal gating behavior in K(+) channels. Nat Struct Mol Biol 18:67–74. doi:10.1038/nsmb.1968

Cuello LG, Jogini V, Cortes DM et al (2010a) Structural basis for the coupling between activation and inactivation gates in K + channels. Nature 466:272–277. doi:10.1038/nature09136

Cuello LG, Jogini V, Cortes DM, Perozo E (2010b) Structural mechanism of C-type inactivation in K + channels. Nature 466:203–207. doi:10.1038/nature09153

Esposito G, Lesk AM, Molinari H et al (1992) Probing protein structure by solvent perturbation of nuclear magnetic resonance spectra. Nuclear magnetic resonance spectral editing and topological mapping in proteins by paramagnetic relaxation filtering. J Mol Biol 224:659–670

Fricke P, Demers J-P, Becker S, Lange A (2013) Studies on the MxiH protein in T3SS needles using DNP-enhanced ssNMR spectroscopy. ChemPhysChem 15:57–60. doi:10.1002/cphc.201300994

Gallagher FA, Kettunen MI, Day SE et al (2008) Magnetic resonance imaging of pH in vivo using hyperpolarized 13C-labelled bicarbonate. Nature 453:940–943. doi:10.1038/nature07017

Gelis I, Vitzthum V, Dhimole N et al (2013) Solid-state NMR enhanced by dynamic nuclear polarization as a novel tool for ribosome structural biology. J Biomol NMR 56:85–93. doi:10.1007/s10858-013-9721-2

Hall DA, Maus DC, Gerfen GJ et al (1997) Polarization-enhanced NMR spectroscopy of biomolecules in frozen solution. Science 276:930–932

Havlin RH, Tycko R (2005) Probing site-specific conformational distributions in protein folding with solid-state NMR. Proc Natl Acad Sci USA 102:3284–3289

Heise H, Luca S, de Groot BL et al (2005) Probing conformational disorder in neurotensin by two-dimensional solid-state NMR and comparison to molecular dynamics simulations. Biophys J 89:2113–2120. doi:10.1529/biophysj.105.059964

Hocking HG, Zangger K, Madl T (2013) Studying the structure and dynamics of biomolecules by using soluble paramagnetic probes. ChemPhysChem 14:3082–3094. doi:10.1002/cphc.201300219

Hohwy M, Rienstra CM, Jaroniec CP, Griffin RG (1999) Fivefold symmetric homonuclear dipolar recoupling in rotating solids: application to double quantum spectroscopy. J Chem Phys 110:7983–7992

Hu K-N, Debelouchina GT, Smith AA, Griffin RG (2011) Quantum mechanical theory of dynamic nuclear polarization in solid dielectrics. J Chem Phys 134:125105. doi:10.1063/1.3564920

Jacso T, Franks WT, Rose H et al (2012) Characterization of membrane proteins in isolated native cellular membranes by

dynamic nuclear polarization solid-state NMR spectroscopy without purification and reconstitution. Angew Chem 124:447–450. doi:10.1002/ange.201104987

Kagawa A, Murokawa Y, Takeda K, Kitagawa M (2009) Optimization of $_1$H spin density for dynamic nuclear polarization using photo-excited triplet electron spins. J Mag Reson 197:9–13. doi:10.1016/j.jmr.2008.11.009

Koers EJ, López-Deber MP, Weingarth M et al (2013) Dynamic nuclear polarization NMR spectroscopy: revealing multiple conformations in lipid-anchored peptide vaccines. Angew Chem Int Ed 52:10905–10908. doi:10.1002/anie.201303374

Lauterbur PC (1973) Image formation by induced local interactions-examples employing nuclear magnetic resonance. Nature 242:190–191. doi:10.1038/242190a0

Linden AH, Franks WT, Akbey Ü et al (2011a) Cryogenic temperature effects and resolution upon slow cooling of protein preparations in solid state NMR. J Biomol NMR 51:283–292. doi:10.1007/s10858-011-9535-z

Linden AH, Lange S, Franks WT et al (2011b) Neurotoxin II bound to acetylcholine receptors in native membranes studied by dynamic nuclear polarization NMR. J Am Chem Soc 133:19266–19269. doi:10.1021/ja206999c

Maly T, Cui D, Griffin RG, Miller A-F (2012) H-1 dynamic nuclear polarization based on an endogenous radical. J Phys Chem B 116:7055–7065. doi:10.1021/jp300539j

Matsuki Y, Takahashi H, Ueda K et al (2010) Dynamic nuclear polarization experiments at 14.1 T for solid-state NMR. Phys Chem Chem Phys 12:5799. doi:10.1039/c002268c

Nadaud PS, Helmus JJ, Höfer N, Jaroniec CP (2007) Long-range structural restraints in spin-labeled proteins probed by solid-state nuclear magnetic resonance spectroscopy. J Am Chem Soc 129:7502–7503. doi:10.1021/ja072349t

Ni QZ, Daviso E, Can TV et al (2013) High frequency dynamic nuclear polarization. Acc Chem Res 46:130425010025008. doi:10.1021/ar300348n

Otting G (2010) Protein NMR using paramagnetic ions. Annu Rev Biophys 39:387–405. doi:10.1146/annurev.biophys.093008.131321

Overhauser AW (1953) Polarization of nuclei in metals. Phys Rev 92:411–415

Pintacuda G, Otting G (2002) Identification of protein surfaces by NMR measurements with a paramagnetic Gd(III) chelate. J Am Chem Soc 124:372–373. doi:10.1021/ja016985h

Reggie L, Lopez JJ, Collinson I et al (2011) Dynamic nuclear polarization-enhanced solid-state NMR of a 13C-labeled signal peptide bound to lipid-reconstituted sec translocon. J Am Chem Soc 133:19084–19086. doi:10.1021/ja209378h

Renault M, Pawsey S, Bos MP et al (2012a) Solid-state NMR spectroscopy on cellular preparations enhanced by dynamic nuclear polarization. Angew Chem Int Ed 51:2998–3001. doi:10.1002/anie.201105984

Renault M, Tommassen-van Boxtel R, Bos MP et al (2012b) Cellular solid-state nuclear magnetic resonance spectroscopy. Proc Natl Acad Sci 109:4863–4868. doi:10.1073/pnas.1116478109

Rosay M, Tometich L, Pawsey S et al (2010) Solid-state dynamic nuclear polarization at 263 GHz: spectrometer design and experimental results. Phys Chem Chem Phys 12:5850–5860. doi:10.1039/c003685b

Rossini AJ, Zagdoun A, Lelli M et al (2013) Dynamic nuclear polarization surface enhanced NMR spectroscopy. Acc Chem Res 46:1942–1951. doi:10.1021/ar300322x

Salnikov E, Rosay M, Pawsey S et al (2010) Solid-state NMR spectroscopy of oriented membrane polypeptides at 100 K with signal enhancement by dynamic nuclear polarization. J Am Chem Soc 132:5940–5941. doi:10.1021/ja1007646

Sauvee C, Rosay M, Casano G et al (2013) Highly efficient, water-soluble polarizing agents for dynamic nuclear polarization at high frequency. Angew Chem Int Ed 52:10858–10861. doi:10.1002/anie.201304657

Schneider R, Ader C, Lange A et al (2008) Solid-state NMR spectroscopy applied to a chimeric potassium channel in lipid bilayers†. J Am Chem Soc 130:7427–7435. doi:10.1021/ja800190c

Sengupta I, Nadaud PS, Helmus JJ et al (2012) Protein fold determined by paramagnetic magic-angle spinning solid-state NMR spectroscopy. Nat Chem 4:410–417. doi:10.1038/nchem.1299

Shen Y, Bax A (2010) SPARTA + : a modest improvement in empirical NMR chemical shift prediction by means of an artificial neural network. J Biomol NMR 48:13–22. doi:10.1007/s10858-010-9433-9

Siemer AB, Huang K-Y, McDermott AE (2012) Protein linewidth and solvent dynamics in frozen solution NMR. PLoS ONE 7:e47242. doi:10.1371/journal.pone.0047242.g001

Smith AA, Corzilius B, Bryant JA et al (2012) A 140 GHz pulsed EPR/212 MHz NMR spectrometer for DNP studies. J Mag Reson 223:170–179. doi:10.1016/j.jmr.2012.07.008

Soares TA, Hünenberger PH, Kastenholz MA et al (2005) An improved nucleic acid parameter set for the GROMOS force field. J Comput Chem 26:725–737. doi:10.1002/jcc.20193

Solomon I (1955) Relaxation processes in a system of two spins. Phys Rev 99:559–565. doi:10.1103/PhysRev.99.559

Takahashi H, Ayala I, Bardet M et al (2013) Solid-state NMR on bacterial cells: selective cell wall signal enhancement and resolution improvement using dynamic nuclear polarization. J Am Chem Soc 135:5105–5110. doi:10.1021/ja312501d

Uysal S, Vasquez V, Tereshko V et al (2009) Crystal structure of full-length KcsA in its closed conformation. Proc Natl Acad Sci USA 106:6644–6649. doi:10.1073/pnas.0810663106

van der Cruijsen EAW, Nand D, Weingarth M et al (2013) Importance of lipid–pore loop interface for potassium channel structure and function. Proc Natl Acad Sci 110:13008–13013. doi:10.1073/pnas.1305563110/-/DCSupplemental

van der Wel PCA, Hu K-N, Lewandowski J, Griffin RG (2006) Dynamic nuclear polarization of amyloidogenic peptide nano-crystals: GNNQQNY, a core segment of the yeast prion protein Sup35p. J Am Chem Soc 128:10840–10846. doi:10.1021/ja0626685

Wang T, Park YB, Caporini MA et al (2013) Sensitivity-enhanced solid-state NMR detection of expansin's target in plant cell walls. Proc Natl Acad Sci USA 110:16444–16449. doi:10.1073/pnas.1316290110

Weingarth M, Prokofyev A, van der Cruijsen EAW et al (2013) Structural determinants of specific lipid binding to potassium channels. J Am Chem Soc 135:3983–3988. doi:10.1021/ja3119114

Weingarth M, van der Cruijsen EAW, Ostmeyer J et al (2014) Quantitative analysis of the water occupancy around the selectivity filter of a K + channel in different gating modes. J Am Chem Soc 136:2000–2007. doi:10.1021/ja411450y

Wickramasinghe NP, Parthasarathy S, Jones CR et al (2009) Nanomole-scale protein solid-state NMR by breaking intrinsic 1H T1 boundaries. Nat Method 6:215–218. doi:10.1038/nmeth.1300

Zachariae U, Schneider R, Velisetty P et al (2008) The molecular mechanism of toxin-induced conformational changes in a potassium channel: relation to C-type inactivation. Structure 16:747–754

Zagdoun A, Casano G, Ouari O et al (2013a) Large molecular weight nitroxide biradicals providing efficient dynamic nuclear

polarization at temperatures up to 200 K. J Am Chem Soc 135:12790–12797. doi:10.1021/ja405813t

Zagdoun A, Rossini AJ, Conley MP et al (2013b) Improved dynamic nuclear polarization surface-enhanced NMR spectroscopy through controlled incorporation of deuterated functional groups. Angew Chem Int Ed 52:1222–1225. doi:10.1002/anie.201208699

Zhou YF, Morais-Cabral JH, Kaufman A, Mackinnon R (2001) Chemistry of ion coordination and hydration revealed by a K + channel-Fab complex at 2.0 angstrom resolution. Nature 414:43–48